Synthesis and Magnetic Properties of Manganese-Doped GaP Nanowires

Doo Suk Han, Seung Yong Bae, Hee Won Seo, Young Joo Kang, and Jeunghee Park*

Department of Chemistry, Korea University, Jochiwon 339-700, Korea

Gangho Lee

Department of Chemistry, Kyungpook National University, Taegu 702-760, Korea

Jae-Pyoung Ahn

Nano-Material Research Center, Korea Institute of Science and Technology, Seoul 136-791, Korea

Soonkyu Kim and Joonyeon Chang

Nano Device Research Center, Korea Institute of Science and Technology, Seoul 130-650, Korea

Received: February 6, 2005; In Final Form: March 11, 2005

We characterized the structure and magnetic properties of Mn-incorporated GaP nanowires synthesized by thermal evaporation of GaP/Mn powders. The nanowires consist of twin-crystalline zinc blende GaP grown with the [111] direction and doped with about 1 at. % Mn. They are often sheathed with the bumpy amorphous outerlayers containing high concentrations of Mn and O. The ferromagnetic hysteresis curves at 5 and 300 K and temperature-dependent magnetization provide evidence for the ferromagnetism with the Curie temperature higher than room temperature. Magnetic properties of individual nanowires have been measured, showing a large negative magnetoresistance equal to about −5% at 5 K. We suggest that the Mn doping of GaP nanowires would form a dilute magnetic semiconductor.

1. Introduction

Diluted magnetic semiconductors (DMSs) are expected to be key materials in future spintronic devices, since they are an excellent media in which charge and spin degrees of freedom are accommodated in a single matter, resulting in interesting magnetic, magnetooptical, magnetoelectronic, and other properties.[1−6] The unique properties of DMSs, such as field-effect control of ferromagnetism, efficient spin injection to produce circularly polarized light, and spin-dependent resonant tunneling, allow technological innovation in magnetoelectronics. Using a theory based on a bound magnetic polaron model, Curie temperatures (T_C) have been calculated for various 5% Mn-doped p-type semiconductors.[5] For (Ga,Mn)As there is great agreement between the theoretical and experimental values of $T_C = 110$ K.[7] The GaN- and ZnO-based DMS materials were predicted to be ferromagnetic with high T_C above room temperature, so they have been extensively studied for many important applications that require the ferromagnetism at room temperature.[8−25] However, many reported experimental values are quite different and even contradictory. Near or above room-temperature ferromagnetism was found by a number of research groups,[8−20] while no ferromagnetism or a very low T_C was also reported.[21−25] Another important III−V DMS, (Ga,Mn)P, had been predicted to have $T_C \approx 100$ K.[5] However, it was reported that the ferromagnetic behaviors can persist at near room temperature for 3 at. % Mn-doped GaP:C films and T_C can depend on the Mn and hole concentrations.[26,27] Therefore the searching for high-T_C DMS materials is still a challenging subject with respect to applications as well as theoretical viewpoints.

Since the discovery of carbon nanotubes,[28] the one-dimensional (1D) semiconductor nanostructures have attracted much attention as well-defined building blocks to fabricate nanoscale electronic and optoelectronic devices.[29,30] The integration of 1D DMS nanostructures into electronics is particularly of importance in order to make real use of the advantages offered by the spins. Recently, the magnetic properties have been investigated for Mn-doped GaN, Co- and Mn-doped ZnO, and Mn-doped GaAs nanowires.[31−35] In this paper, we first report the Mn-incorporated GaP nanowires exhibiting the ferromagnetism at room temperature. We synthesized the nanowires via simple thermal evaporation that was developed for the synthesis of undoped GaP nanowires.[36] The structure, composition and magnetic properties were thoroughly investigated by scanning electron microscopy (SEM), transmission electron microscopy (TEM), high-voltage TEM (HVEM) using 1.25 MV, scanning TEM (STEM) elemental mapping, energy-dispersive X-ray spectroscopy (EDX), high-resolution X-ray diffraction (XRD), Raman spectroscopy, and superconducting quantum interference (SQUID, Quantum Design) magnetometer.

2. Experimental Section

GaP (99.99%, Aldrich) pieces were milled using a mechanical ball mill system for 20 h. The ball-milled GaP and Mn (99.99%, Aldrich) powder mixture was placed in a quartz boat located inside a quartz tube reactor. Silicon substrates were coated with a 0.01 M $HAuCl_4 \cdot 3H_2O$ (98+%, Sigma) ethanol solution, leading to the deposition of Au nanoparticles. The substrate was

* Corresponding author. E-mail: parkjh@korea.ac.kr.

10.1021/jp050655s CCC: $30.25
Published on Web 04/13/2005

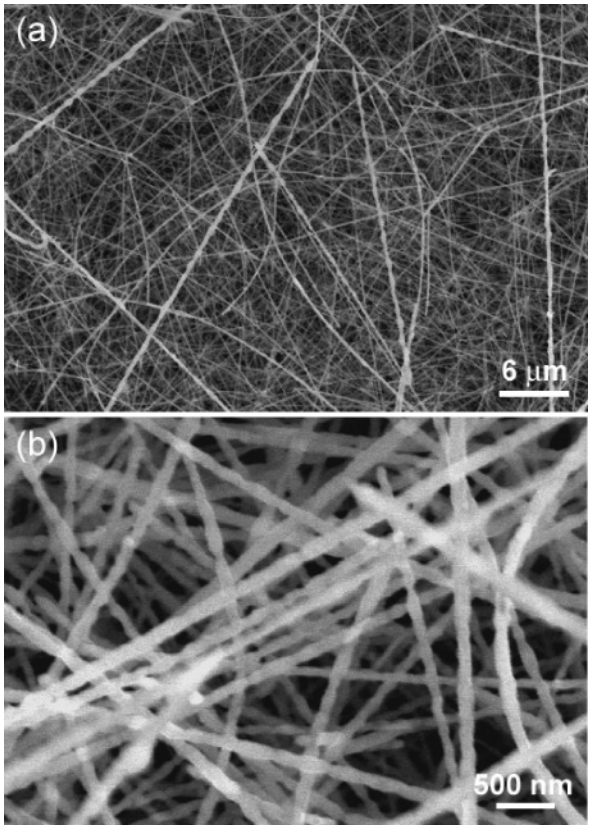

Figure 1. (a) SEM micrograph for high-density nanowires homogeneously grown on the substrate. (b) Magnified image reveals the bumpy surface of the nanowires.

placed at a distance of about 15 cm from the boat. The source was sublimated under the Ar flow with a rate of 500 cm^3(STP) min^{-1}. The temperature of the GaP source was set at 1100 °C, and that of the substrate was approximately 800−850 °C. The growth time was 10 min. Bright-yellow colored product was deposited on a large area of the substrate. SEM (Hitachi S-4300), TEM (JEOL JEM-2010), and HVEM (JEOL, JEM ARM 1300 S, 1.25 MV), electron diffraction (ED), STEM attached to TEM (FEI TECNAI G^2), and Raman spectroscopy (Renishaw RM1000) using 514.5 nm were employed. XRD patterns were measured using the 8C2 beam line of the Pohang Light Source (PLS) with monochromatic radiation (λ = 1.5403 Å). Magnetic properties of samples were studied by SQUID (Quantum Design) magnetometer.

3. Results and Discussion

SEM micrographs show that high-density nanowires were grown homogeneously on a large area of the substrates (Figure 1a). The average length is about 100 μm. A magnified image reveals the bumpy surface of the nanowires (Figure 1b).

A TEM image for the general morphology of the nanowires is displayed in Figure 2a. The nanowires have nearly even or periodically bumpy surface along the wire axis. Few catalytic nanoparticles attach to the end of the nanowires. The diameter of the nanowires is in the range 40−100 nm. The bumpy nanowires have usually a larger diameter than the smooth nanowires. The HVEM image of the smooth nanowires shows exclusively the twin structure of the defect lines that exist between the single-crystalline zinc blende structured GaP crystal domains, perpendicularly to the wire axis (Figure 2()). The (111) plane fringes are separated by about 3.1 Å, which is consistent with that of zinc blende GaP (a = 5.4506 Å; JCPDS Card No. 32-0397). The inset is a fast Fourier transformed (FFT) ED pattern, corresponding to that of a twin-crystalline zinc blende GaP crystal. The growth direction is [111], which is the same as that of undoped GaP nanowires.[36] The detailed feature of the bumpy nanowires is displayed in Figure 2c. The nanowire core is sheathed with the bumpy amorphous outerlayers. Figure 2d corresponds to atomic-resolved HVEM image for the marked area in Figure 2c, revealing a number of twins in the crystalline GaP crystal. The growth direction is [111], and the defect lines are usually formed along the [111] direction. HVEM image for the bumpy part shows that most of them are in amorphous phase and there are some embedded GaP nanosize crystals. The significant twin structures and the bumpy outer layers were never found in the undoped GaP nanowires, so their formation must be related with the Mn incorporation.

Figure 3 corresponds to the STEM elemental mapping of Ga, P, Mn, and O concentrations in the bumpy nanowire. The bright points indicate the high concentration of the elements, showing that the Mn distributes inhomgeneously and concentrates at the bumpy parts. Ga and P consist of the nanowire core part with the ratio of about 1 (Figure 3a,b). The bumpy outer layers contain the higher Mn and O concentrations than the nanowire part (Figure 3c,d). The cross-sectional elemental mapping confirms that the outer layers mainly consist of Mn and O (Figure 3e). The corresponding STEM image is shown in the inset. The content of the Mn/(Ga + Mn) atom percent is determined to be about 20 at. % for the outer-layer parts. From the EDX data of many smooth or bumpy nanowires, we estimated the average Mn content to be 10 at. % for the amorphous bumpy parts and 1 at. % for the crystalline nanowire parts (Figure S1c).

The higher amount of Mn content at the bumpy part can be explained by the vapor−liquid−solid growth mechanism. The GaP and Mn vapors dissolve in the Au catalytic nanoparticles and then precipitate simultaneously after the saturation. It is known that the solubility of Mn in Au metal is less than that of Ga.[37] The excess Mn vapor that cannot dissolve in the Au nanoparticles due to a limited solubility may deposit as amorphous oxide layers on the surface of the growing GaP nanowire core.

The XRD pattern has been measured for the undoped and Mn-doped GaP nanowires, showing a typical one of a zinc blende GaP crystal (Figure 4a). The undoped GaP nanowires were synthesized by the procedure described previously.[36] Other possible Ga−Mn, Mn−O, or Mn−P composition crystalline phases were not detected. Figure 4b shows the first-order Raman spectrum of Mn-doped GaP nanowires. It shows only first-order phonon frequencies of transverse optical (TO) and longitudinal optical (LO) modes of GaP at 367 and 400 cm^{-1}, respectively, which is consistent with the reported values of zinc blende GaP as well as undoped GaP nanowires whose Raman spectrum is displayed in the same figure.[36,38] Recently, a peak on the left side of the LO mode peak was assigned to surface phonon (SP) mode of GaP nanowires.[39,40] It was suggested that the frequency is sensitive to the dielectric constant of the surrounding medium in which the nanowire is imbedded. The Mn-doped GaP nanowires show the significant SP mode peak at 385 cm^{-1}, which could be related to the amorphous outer layers as well as many defects in the twin-crystalline GaP.

The magnetization (M) vs magnetic field (H), measured by SQUID magnetometry, is shown in Figure 5. To eliminate the signals from the substrates, the nanowires are separated from the substrates. A nonlinearity in M is observed with an obvious amount of hysteresis at 5 and 300 K. The ferromagnetism is

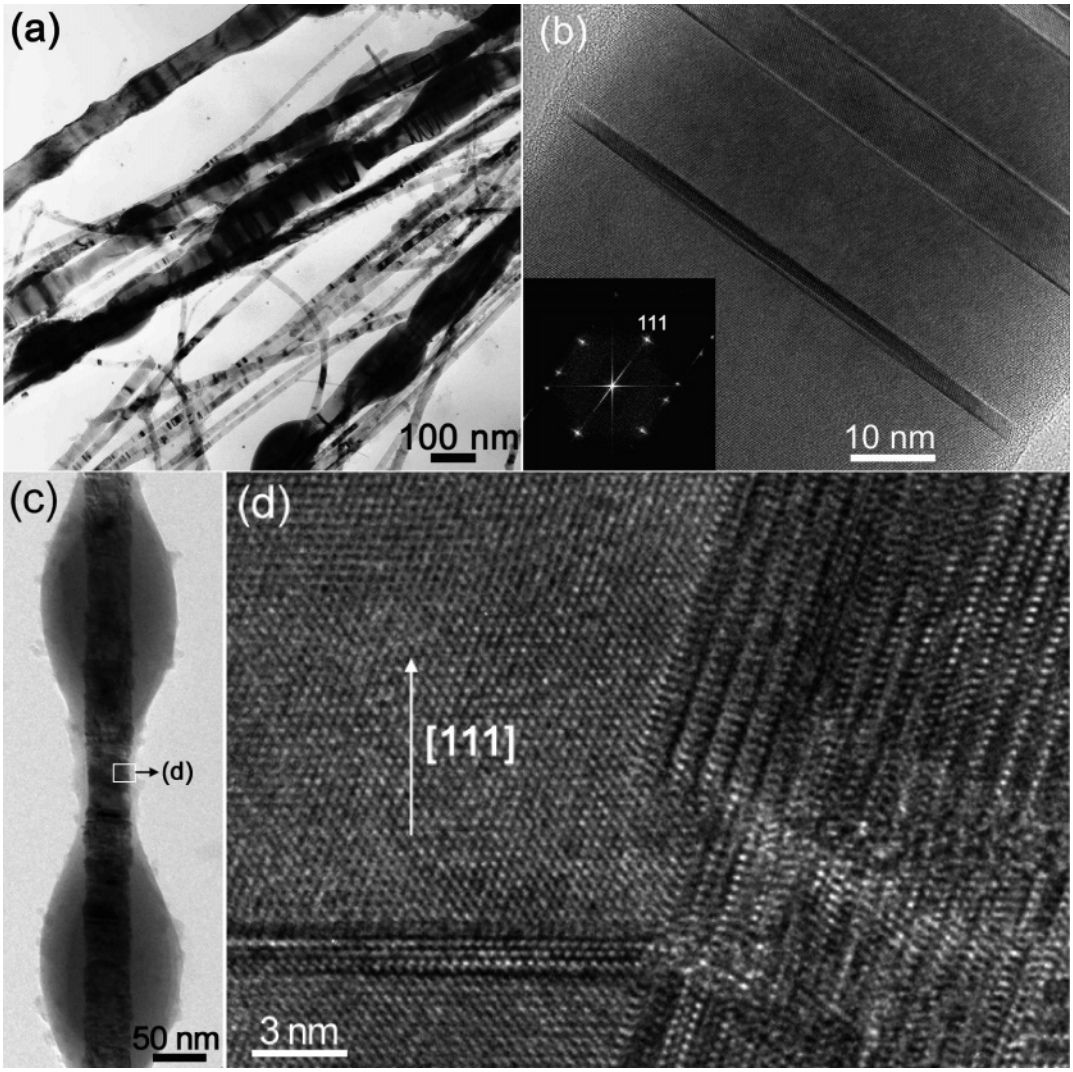

Figure 2. (a) TEM image showing the typical morphology of Mn-doped GaP nanowires. The diameter is 40−100 nm. (b) A smooth nanowire has highly crystalline lattice planes with a few defect lines perpendicular to the growth direction. The inset corresponds to the FFT ED pattern, showing the [111] growth direction. (c) Detailed feature of a bumpy nanowire and its (d) atomic-resolved HVEM image showing a number of defect lines along the [111] direction.

clearly shown by coercivity, remanence, and relatively low saturation field. At 300 K, the coercivity and remanence of hysteresis become smaller, which may be due to the intrinsic magnetically soft properties, but the loop still shows the features of ferromagnetism. Figure 5b displays the difference $\Delta M = M_{FC} - M_{ZFC}$ magnetization curve measured with $H = 100$ Oe, as a function of temperature. The FC and ZFC magnetization curves measured as a function of temperature are displayed in the inset. The FC − ZFC subtraction is particularly effective when there are small amounts of ferromagnetic material in the presence of diamagnetic and/or paramagnetic background. Thus the subtraction indicates the presence of hysteresis if the difference is nonzero. The ΔM vs T curve shows that the ferromagnetism can persist up to 330 K.

With regard to the origin of the ferromagnetic component in our samples, one of the possibilities is the existence of nanosized MnO or Mn_3O_4 impurities in the outer layers. The MnO nanocrystals with diameters of 5−22 nm were reported to have $T_C = 27-10$ K, and the Mn_3O_4 nanocrystals with diameters of 6−15 nm have $T_C = 36-41$ K, so they may not contribute in our high T_C.[41,42] Other possible ferromagnetic impurities MnP and GaMn crystallites have $T_C = 291$ K and >300 K, respectively.[43,44] Although the HVEM and XRD data do not provide any evidence for their presence in our sample, we may not rule them out as a potential source considering the detection limits. Before drawing further convincing evidence for MnP or GaMn, we tentatively propose that the 1% Mn doping of the GaP crystal would lead to the formation of a DMS material having $T_C > 300$ K. However, the T_C is anomalously higher than the theoretically predicted $T_C = 100$ K of 5% Mn-doped p-type GaP.[5] Theodoropoulou et al. reported that the Mn-doped GaP film shows a dependence of T_C on the Mn concentration, and a maximum $T_C = 270$ K for 3% Mn doping on the hole-doped substrates, which has been explained by the contribution of the disorder of spin clusters.[26] Our high T_C value is nearly consistent with that of the Mn-doped GaP film.

To examine the magnetic properties of an individual nanowire, the magnetoresistance (MR) was measured by the following procedure. The Mn-doped GaP nanowires were dropped onto the Si substrate with a 200 nm thick thermally grown SiO_x layer that the alignment marks had been made. The electrical leads were defined using electron beam lithography on the selected nanowire. For ohmic contact, 20 nm of Ni and 50 nm of Au films deposited on the contact area by electron beam evaporation and followed by rapid thermal annealing for 1 min at 500 °C. Figure 6a shows the SEM image of a single bumpy nanowire connected with four electrodes. The distance between the electrodes is about 850 nm. The formation of stable electrical

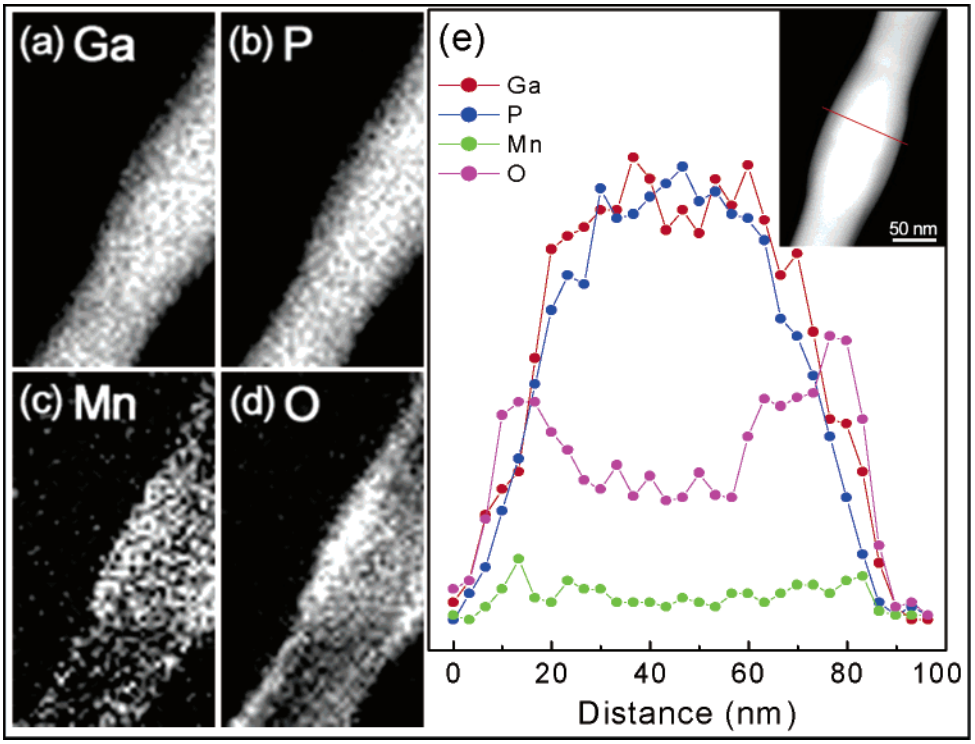

Figure 3. STEM elemental maps of (a) Ga, (b) P, (c) Mn, and (d) O concentrations in a bumpy nanowire, and (e) elemental mapping cross-section showing that Mn and O concentrates at the outer layers. The corresponding STEM image is shown in the inset.

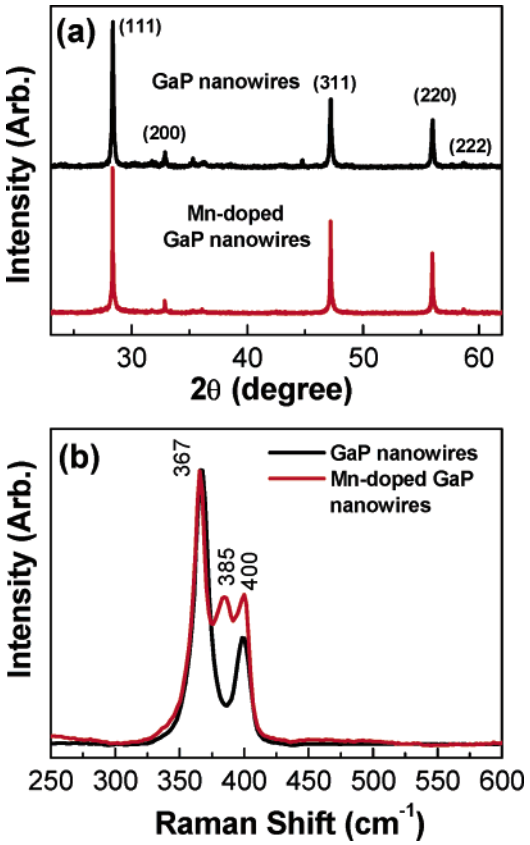

Figure 4. (a) Full-range XRD pattern of GaP and Mn-doped GaP nanowires. (b) Raman scattering spectrum of GaP and Mn-doped GaP nanowires. The excitation wavelength is 514.5 nm from argon ion laser.

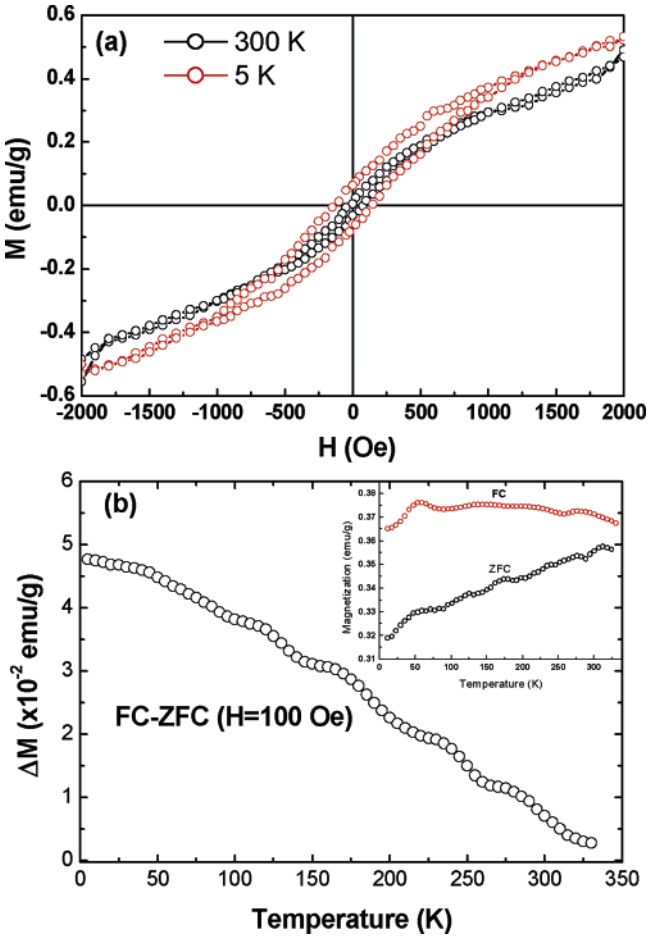

Figure 5. (a) M vs H curves at 5 and 300 K, and (b) temperature-dependent $\Delta M = M_{FC} - M_{ZFC}$ measured with $H = 100$ Oe. The inset displays the M_{FC} and M_{ZFC} curves.

contacts was confirmed to ensure consistent measurements. Magnetotransport properties were monitored by sweeping the magnetic field up to ±9 T perpendicular to the substrates, in the temperature range between 5 and 200 K. The MR ratio is defined as MR = $[R(H) - R(0)]/R(0) \times 100\%$, where $R(H)$ is the resistance at field H and $R(0)$ is the maximum resistance at

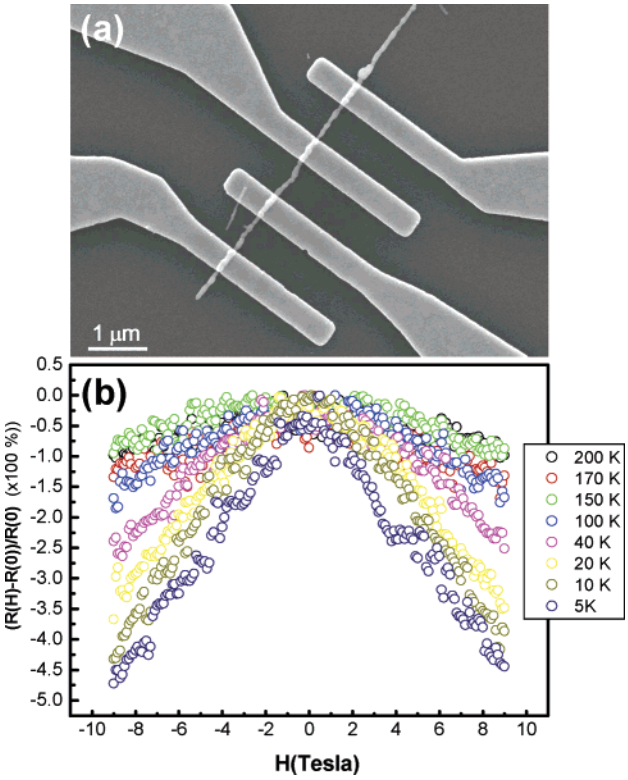

Figure 6. (a) SEM image of a nanowire attached to four electrodes. (b) MR at various temperatures in the range 5−200 K, for magnetic field sweeps between −9 and +9 T.

the zero applied field, at each temperature. The temperature-dependent resistance follows a typical resistance change of semiconductor. The current−voltage ($I-V$) curves (not presented) show linear relationship in the voltage range of 0−2 V at room temperature, indicating good ohmic contact. Therefore, the MR has been measured under no bias voltage dependence. With $H = \pm 9$ T the Mn-doped GaP nanowire shows a maximum negative MR equal to about 5% at 5 K, as in Figure 6b. The negative MR persists until 200 K. Such negative MR behavior below 200 K has been also found in the Mn-doped GaP films.[27] The MR value is only −0.35% at 20 K. Our MR value at 20 K is 10 times larger than that of the film. The observed negative MR can be understood as the reduction of scattering by the aligning spins under the applied magnetic field. The negative MR of (In,Mn)As and (Ga,Mn)As films was explained by the mechanism that the formation of bound magnetic polarons, and the increase of Fermi energy in a spin split band result in the reduction of the localization length that determines the energy difference between the mobility edge and the Fermi level.[7,45] The remarkably large MR value of the Mn-doped GaP nanowires implies the efficient alignment of spins along the long axis of the nanowires. More studies will be necessary to verify the origin of high T_C and large negative MR values. Nevertheless unique magnetic properties of Mn-doped GaP nanowires promise a great potential for the applications in nanospintronics.

4. Conclusion

The Mn-doped GaP nanowires were synthesized by thermal evaporation of ball-milled GaP and Mn powders. The diameter is 40−100 nm. The nanowires are frequently sheathed with the bumpy amorphous outer layers. The HVEM images reveal a high degree of twin structure in the zinc blende GaP crystal grown with the [111] direction. The STEM elemental mapping reveals the inhomogeneous Mn doping concentrated at the amorphous outer layers. Average Mn content is estimated to be about 1 at. % for the nanowire parts and about 10 at. % for the outer layers. The amorphous outer layers mainly consist of Mn and O. The XRD pattern and Raman spectroscopy confirm that the nanowires have only zinc blende GaP crystals. The hysteresis curves measured at 5 and 300 K, and the temperature-dependent magnetization curves with $H = 100$ Oe provide an evidence for the ferromagnetism with T_C higher than 330 K. The magnetotransport properties of individual nanowires have been measured in the temperature range 5−200 K, showing the large negative MR at temperatures over this range. The absolute value of MR percent reaches to about 5% at 5 K. We suggest that Mn would efficiently dope into the GaP nanowires and form the DMS nanowires. These Mn-doped GaP nanowires would be encouraging ferromagnetic semiconductor nanowires applicable to the spintronic nanodevices.

Acknowledgment. This work was supported by KOSEF (Project No. R14-2004-033-01003-0; R02-2004-000-10025-0) and KRF (Project No. 2004-015-C00125). SEM, HVEM, and SQUID measurements were performed at Basic Science Research Center. Experiments at PLS were supported in part by MOST and POSTECH.

Supporting Information Available: Figure S1, showing the EDX data of Mn-doped GaP nanowires (PDF). This material is available free of charge via Internet at http://pubs.acs.org.

References and Notes

(1) Ohno, H. *Science* **1998**, *281*, 951.
(2) Fiederling, R.; Keim, M.; Reuscher, G.; Ossau, W.; Schmidt, G.; Waag, A.; Molenkamp, L. W. *Nature (London)* **1999**, *402*, 787.
(3) Ohno, Y.; Young, D. K.; Beschoten, B.; Matsukura, F.; Ohno, H.; Awschalom, D. D. *Nature (London)* **1999**, *402*, 790.
(4) Ohno, H.; Chiba, D.; Matsukura, F.; Omiya, T.; Abe, E.; Dietl, T.; Ohno, Y.; Ohtani, K. *Nature (London)* **2000**, *408*, 944.
(5) Dietl, T.; Ohno, H.; Matsukura, F.; Cibert, J.; Ferrand, D. *Science* **2000**, *287*, 1019.
(6) Wolf, S. A.; Awschalom, D. D.; Buhrman, R. A.; Daughton, J. M.; von Molnár, S.; Roukes, M. L.; Chtchelkanova, A. Y.; Treger, D. M. *Science* **2001**, *294*, 1488.
(7) Ohno, H.; Matsukura, F. *Solid State Commun.* **2001**, *117*, 179.
(8) Theodoropoulou, N.; Hebard, A. F.; Overberg, M. E.; Abernathy, C. R.; Pearton, S. J.; Chu, S. N. G.; Wilson, R. G. *Appl. Phys. Lett.* **2001**, *78*, 3475.
(9) Reed, M. L.; El-Mastry, N. A.; Stadelmaier, H. H.; Ritums, M. K.; Reed, M. J.; Parker, C. A.; Roberts, J. C.; Bedair, S. M. *Appl. Phys. Lett.* **2001**, *79*, 3473.
(10) Sasaki, T.; Sonoda, S.; Yamamoto, Y.; Suga, K.; Shimizu, S.; Kindo, K.; Hori, H. *J. Appl. Phys.* **2002**, *91*, 7911.
(11) Sardar, K.; Raju, A. R.; Bansal, B.; Venkataraman, V.; Rao, C. N. R. *Solid State Commun.* **2003**, *125*, 55.
(12) Lee, J. M.; Lee, K. I.; Chang, J. Y.; Ham, M. H.; Huh, K. S.; Myung, J. M.; Hwang, W. J.; Shin, M. W.; Han, S. H.; Kim, H. J.; Lee, W. Y. *Microelectron. Eng.* **2003**, *69*, 283.
(13) Yoon, I. T.; Park, C. S.; Kim, Y. G.; Kang, T. W.; Jeong, M. C.; Ham, M. H.; Myoung. J. M. *J. Appl. Phys.* **2004**, *95*, 591.
(14) Giraud, R.; Kuroda, S.; Marcet, S.; Bellet-Amalric, E.; Biquard, X.; Barbara, B.; Frauchart, D.; Ferrand, D.; Cibert, J.; Mariette, H. *Europhys. Lett.* **2004**, *65*, 553.
(15) Ueda, K.; Tabata, H.; Kawai, T. *Appl. Phys. Lett.* **2001**, *79*, 988.
(16) Cho, Y. M.; Choo, W. K.; Kim, H.; Kim, D.; Ihm, Y. *Appl. Phys. Lett.* **2002**, *80*, 3358.
(17) Lee, H.-J.; Jeong, S.-Y.; Cho, C. R.; Park, C. H. *Appl. Phys. Lett.* **2002**, *81*, 4020.
(18) Han, S.-J.; Song, J. W.; Yang, C.-H.; Park, S. H.; Park, J.-H.; Jeong, Y. H.; Rhie, K. W. *Appl. Phys. Lett.* **2002**, *81*, 4212.
(19) Norton, D. P.; Pearton, S. J.; Hebard, A. F.; Theodoropolou, N.; Boatner, L. A.; Wilson, R. G. *Appl. Phys. Lett.* **2003**, *82*, 239.
(20) Yan, S.; Ren, C.; Wang, X.; Xin, Y.; Zhou, Z. X.; Mei, L. M.; Ren, M. J.; Chen, Y. X.; Liu, Y. H.; Garmestani, H. *Appl. Phys. Lett.* **2004**, *84*. 2376.
(21) Zajac, M.; Doradzinski, R.; Gosk, J.; Szczytko, J.; Lefeld-Sosnowska, M.; Kaminska, M.; Twardowski, A.; Palczewska, M.; Grzanka, E.; Gebicki, W. *Appl. Phys. Lett.* **2001**, *78*, 1276.

(22) Overberg, M. E.; Abernathy, C. R.; Pearton, S. J.; Theodoropoulou, N. A.; McCarthy, K. T.; Hebard, A. F. *Appl. Phys. Lett.* **2001**, *79*, 1312.
(23) Fukumura, T.; Jin, Z.; Ohtomo, A.; Koinuma, H.; Kawasaki, M. *Appl. Phys. Lett.* **1999**, *75*, 3366.
(24) Jin, Z.; Fukumura, T.; Kawasaki, M.; Ando, K.; Saito, H.; Sekiguchi, T.; Yoo, Y. Z.; Murakami, M.; Matsumoto, Y.; Hasegawa, T.; Koinuma, H. *Appl. Phys. Lett.* **2001**, *78*, 3824.
(25) Jung, S. W.; An, S.-J.; Yi, G.-C.; Jung, C. U.; Lee, S.-I.; Cho, S. *Appl. Phys. Lett.* **2002**, *80*, 4561.
(26) Theodoropoulou, N.; Hebard, A. F.; Overberg, M. E.; Abernathy, C. R.; Pearton, S. J.; Chu, S. N. G.; Wilson, R. G. *Phys. Rev. Lett.* **2002**, *89*, 107203.
(27) Overberg, M. E.; Gila, B. P.; Abernathy, C. R.; Pearton, S. J.; Theodoropoulou, N. A.; McCarthy, K. T.; Arnason, S. B.; Hebard, A. F. *Appl. Phys. Lett.* **2001**, *79*, 3128.
(28) Iijima, S. Nature **1991**, *354*, 56.
(29) Duan, X.; Huang, Y.; Cui, Y.; Wang, J.; Lieber, C. M. *Nature* **2001**, *409*, 66.
(30) Duan, X.; Huang, Y.; Agarwal, R.; Lieber, C. M. *Nature* **2003**, *421*, 241.
(31) Han, D. S.; Park, J.; Rhie, K. W.; Kim, S.; Chang, J. *Appl. Phys. Lett.* **2005**, *86*, 032506.
(32) Deepak, F. L.; Vanitha, P. V.; Govindaraj, A.; Rao, C. N. R. *Chem. Phys. Lett.* **2003**, *374*, 314.
(33) Wu, J. J.; Liu, S. C.; Yang, M. H. *Appl. Phys. Lett.* **2004**, *85*, 1027.
(34) Chang, Y. Q.; Wang, D. B.; Luo, X. H.; Xu, X. Y.; Chen, X. H.; Li, L.; Chen, C. P.; Wang, R. M.; Xu, J.; Yu, D. P. *Appl. Phys. Lett.* **2003**, *83*, 4020.
(35) Jeon, H. C.; Chung, K. J.; Chung, K. J.; Kang, T. W.; Kim, T. W. *Jpn. J. Appl. Phys.* **2004**, *43*, L963.
(36) Seo, H. W.; Bae, S. Y.; Park, J.; Yang, H.; Kim, S. *Chem. Commun.* **2002**, 2564.
(37) Massalski, T. B. *Binary Alloy Phase Diagrams*; American Society for Metals: Metals Park, OH, 1986.
(38) Nasibov, A. S.; Mel'nik, N. N.; Ponomarev, I. V.; Romanko, S. V.; Topchii, S. B.; Braztsov, A. N.; Yu Bashtanov, M.; Krasnovskii, A. A. *Quantum Electron.* **1998**, *28*, 40.
(39) Gupta, R.; Xiong, Q.; Mahan, G. D.; Eklund, P. C. *Nano Lett.* **2003**, *3*, 1745
(40) Mahan, G. D.; Gupta, R.; Xiong, Q.; Adu, C. K.; Eklund, P. C. *Phys. Rev. B* **2003**, *68*, 073402.
(41) Lee, G. H.; Huh, S. H.; Jeong, J. W.; Choi, B. J.; Kim, S. H.; Ri, H.-C. *J. Am. Chem. Soc.* **2002**, *124*, 12094.
(42) Seo, W. S.; Jo, H. H.; Lee, K.; Kim, B.; Oh, S. J.; Park, J. T. *Angew. Chem., Int. Ed.* **2004**, *43*, 1115.
(43) Shapira, Y.; Oliveira, N. F., Jr.; Becerra, C. C.; Foner, S. *Phys. Rev. B* **1984**, *29*, 361.
(44) Tanaka, M.; Harbison, J. P.; DeBoeck, J.; Sands, T.; Phillips, B.; Cheeks, T. L.; Keramidas, V. G. *Appl. Phys. Lett.* **1993**, *62*, 1565.
(45) Ohno, H.; Munekata, H.; Penney, T.; von Molnár, S.; Chang, L. L. *Phys. Rev. Lett.* **1992**, *68*, 2664.